Available online at www.sciencedirect.com
ScienceDirect
Trans. Nonferrous Met. Soc. China 35(2025) 431−445
Transactions of Nonferrous Metals Society of China
www.tnmsc.cn

Synergistic effect of low Gd+Mn additions on evolution of microstructure and mechanical properties of Mg−Gd−Mn alloy

Dong-dong GU[1,2], Jian PENG[1], Fu-sheng PAN[1]

1. National Engineering Research Center for Magnesium Alloys, College of Materials Science and Engineering, Chongqing University, Chongqing 400044, China;
2. College of Mechanical and Electrical Engineering, Jinggangshan University, Jinggangshan 343009, China

Received 29 June 2023; accepted 28 February 2024

Abstract: The synergistic effect of low Gd+Mn additions on the evolution of microstructure and mechanical properties of Mg−*x*Gd−0.8Mn alloy was investigated. Gd addition shows a strong grain refinement effect on the extruded Mg−*x*Gd−0.8Mn alloy, and leads to a continuous decrease in the area fraction of basal texture grains and the corresponding maximum density of texture components. However, the maximum density of the basal texture components grows abruptly as Gd content increases to 6 wt.%. When the Gd content is below 6 wt.%, the asymmetry of the tensile and compressive yield of the alloy is negatively correlated to the Gd content due to grain refinement and texture weakening effects. Besides, the contribution of grain refinement to higher alloy yield strength is more significant than that of grain orientation. Compared with the extruded Mg−*x*Gd alloy, the extruded Mg−*x*Gd−0.8Mn alloy shows a lower limit composition point that corresponds to solid solution strengthening and plasticizing effect (2 wt.% and 4 wt.%). Finally, the trend of basal slip and prismatic slip resistance variations of the extruded Mg−*x*Gd−0.8Mn alloys was predicted.

Key words: Mg−Gd−Mn alloy; Gd+Mn additions; mechanical properties; texture evolution; solid solution strengthening and plasticizing effect

1 Introduction

Magnesium alloys demonstrate advantageous performances (such as low density) and excellent application potential in numerous fields that demand lightweight materials and energy conservation [1−3]. However, deformed magnesium alloys show poor plasticity and formability due to their HCP crystal structure and low stacking fault energy, which limits their application scope [4,5].

Alloying is an effective approach to adjust the microstructure and mechanical properties of metallic materials. Gd, a rare earth element which is abundant in nature and demonstrates high matrix solid solubility, is a promising alloying material to improve the strength and plasticity of magnesium alloys [6−12]. Despite that dilute Mg−Gd alloy has a large grain size and medium-strength texture, it still exhibits remarkable plasticity. Gd can promote the activation of non-basal slip systems, thereby providing more effective paths for dislocation movement and improving the plasticity of Mg alloys by weakening the metallic texture [8]. Gd atomic solid solution can suppress the transition of the slip from a non-basal to basal status when provided at an appropriate amount, resulting in sufficient ⟨*c*+*a*⟩ dislocation inside the alloy, which is a prerequisite for cross slip. However, excessive Gd addition will lead to significant solid solution

Corresponding author: Jian PENG, Tel: +86-23-65112291, E-mail: jpeng@cqu.edu.cn
DOI: https://doi.org/10.1016/S1003-6326(24)66690-2

strengthening and second phase strengthening. Besides, the texture of the alloy may transform from a rare earth texture to a basal texture, which may bring lower alloy plasticity and higher cost [6]. Therefore, the optimal approach to decrease Gd addition while not damaging the strength and plasticity of the alloy has been a recent hot spot for research [12−15].

HARMUTH et al [16] reported that the mechanical properties of Mg−Gd alloy can be tailored across a wide range by solid solution strengthening, texture changes and slip activities. In our previous studies, we identified that the optimal Gd content in the extruded Mg−Gd alloy for optimal plasticity is around 4 wt.%, which is consistent with the results obtained by HU et al [11]. The structure and properties of the Mg−Gd alloy can be further regulated for efficient utilization of alloying elements. Specifically, low-cost Mn is often combined with Gd to improve the alloy mechanical properties [3,17−19]. With Mn addition, metal grains are refined further with a higher degree of recrystallization [18]. Besides, Mn addition may not only reduce the atomic loss of Gd during impurity removal processes and improve the alloying efficiency of Gd, but also have the potential in developing Mg alloy with excellent properties [20,21]. However, research on the effect of low Gd content and Mn addition on the microstructure and mechanical properties, such as changes in the elemental composition and the alloy plasticization effect, remains quite limited.

This work aims to explore the influence of Gd addition (0, 2, 4, and 6 wt.%) on the microstructure, texture, and mechanical properties of Mg−*x*Gd−0.8Mn alloy and discuss the correlation between the microstructure and mechanical properties. In addition, a comparative study is performed to find the effective range of Gd addition that produces solid solution plasticization effects in the extruded Mg−*x*Gd and Mg−*x*Gd−0.8Mn alloys.

2 Experimental

Master alloys (Mg−25%Gd and Mg−3.25%Mn (mass fraction)) and commercially pure Mg (99.97%) were used to prepare the Mg−*x*Gd−0.8Mn alloy (*x*=0, 2, 4, and 6 wt.%) in a low carbon steel crucible under the shielding gas (CO_2:SF_6=99:1, vol.%). Pure Mg was placed in a low carbon steel crucible (*d* 85 mm) at room temperature. The pure Mg was heated until it was fully melted, and then Mg−Gd and Mg−Mn master alloys were added sequentially at 780 and 820 °C, respectively. Upon the addition of all raw materials, the temperature was adjusted to 720 °C, and held for 30 min, and then quickly immersed the mixture with the crucible in cold water to obtain the alloy ingot. Subsequently, the Mg−*x*Gd−0.8Mn alloy ingots were subject to a two-stage heat treatment of 350 °C for 6 h followed by 510 °C for 18 h. The actual composition of ingots was tested by inductively coupled plasma-atomic emission spectroscopy (ICP-AES) with a testing accuracy of 3×10^{-6} and an error smaller than 2×10^{-6} (Table 1). After preheating at 430 °C for 1 h, the 5 mm × 60 mm alloy sheets were extruded at 430 °C with an extrusion ratio of 19:1.

Table 1 Nominal and actual chemical composition of alloys

Nominal composition/wt.%	Actual composition/wt.%			
	Mn	Gd	Si	Mg
Mg−0.8Mn	0.82	0	0.0151	Bal.
Mg−2Gd−0.8Mn	0.81	2.23	0.0150	Bal.
Mg−4Gd−0.8Mn	0.88	3.99	0.0178	Bal.
Mg−6Gd−0.8Mn	0.86	5.99	0.0137	Bal.

In this study, cast samples were taken from the center of the ingot and at 1/2 of the radius, while extruded samples were obtained from the center of the sheet (ED−TD plane). These samples for microstructural observation were wet ground to a 1200 grit-finish by a SiC paper and etched with an etchant (cast samples: alcohol solution with 4% nitric acid; extruded samples: 5 g picric acid + 5 g acetic acid + 10 mL distilled water + 100 mL anhydrous ethanol). After that, the samples were characterized by optical microscopy (OM, ZEISS Axiovert 40 MAT) and observed under a scanning electron microscope (SEM, Tescan Vega 3 LMH) equipped with an energy dispersive X-ray spectroscopy (EDS). The phases of the as-cast alloy were identified by X-ray diffraction (Rigaku D/MAX−2500PC). The ED−ND plane of the extruded samples was mechanically polished and electro-polished prior to characterization with electron backscatter diffraction (EBSD, JEOLJSM−7800F). Besides, an eddy current conductivity

meter (Sigmascope SMP10) was implemented to test the electrical conductivity of the alloy more than 10 times and evaluate the solubility of the solid solute. Tensile and compressive specimens were cut from the extruded plate parallel to the ED direction following the GB/T228—2002 standard (gauge length, width, and thickness for the tensile specimen: 21 mm × 5 mm × 3 mm; for the compressive specimen: 7.5 mm × 5 mm × 5 mm). The tensile and compressive tests were conducted at room temperature on a CMT5105 universal testing machine with a strain rate of 2 mm/min. Each alloy condition was tested in triplicates for tensile and compressive strength to ensure data accuracy.

3 Results

3.1 Microstructure

Figure 1 shows the OM and SEM images of the as-cast Mg−*x*Gd−0.8Mn (*x*=0, 2, 4, and 6 wt.%) alloys. All alloy samples contain interdendritic regions that consist of dendritic grains and eutectic compounds, and the dendrite spacing and number of dendrite units gradually decrease with higher Gd content. When Gd is not present, Mg−0.8Mn alloy exhibits relatively coarse grain size (average grain size ~1277.4 μm). As the content of Gd grows to 2, 4, and 6 wt.%, the alloy grains are gradually refined to smaller average grain sizes of 963.0, 885.2 and 527.8 μm, respectively. According to Figs. 1(e−h), the second phases are mainly distributed at the boundary of the alloy dendrites with their volume fraction positively correlated to higher Gd content. Judging from the XRD patterns (Fig. 2) and EDS results (Table 2), Mg−0.8Mn alloy comprises *α*-Mg, Mg_2Si and Mn phases. Following Gd addition, the second phases mainly include the *α*-Mg, Mg_5Gd, Mg_2Si, and Mn phases. Mg_2Si phase is formed because Si is present as an impurity in the alloy. Based on these results, Mn will not form any new phases with Mg or Gd. However, EDS analysis of the second phase suggests that Mn and Gd can coexist, indicating that Mn atoms may dissolve in the Mg_5Gd phase [17].

Figure 3 shows the micrographs and grain size distribution of the extruded Mg−*x*Gd−0.8Mn alloy sheets. All these alloy sheets undergo complete dynamic recrystallization after extrusion deformation with microstructures of uniform and refined equiaxed grains, which are significantly refined compared to the cast alloy. The extruded Mg−0.8Mn alloy exhibits unusually coarse grains with an average size of 23.95 μm. The presence of 2 wt.% Gd results in a significant decrease of the grain size to 7.06 μm. However, further addition of Gd to 4 wt.% and 6 wt.% only leads to insignificant drop of the grain size to 6.97 and 6.17 μm, respectively. In extruded alloys, the solid solubility of Gd atoms in the Mg matrix and the solute segregation at grain boundaries are limited, which would not continuously and efficiently hinder the migration of grain boundaries. In addition, effective

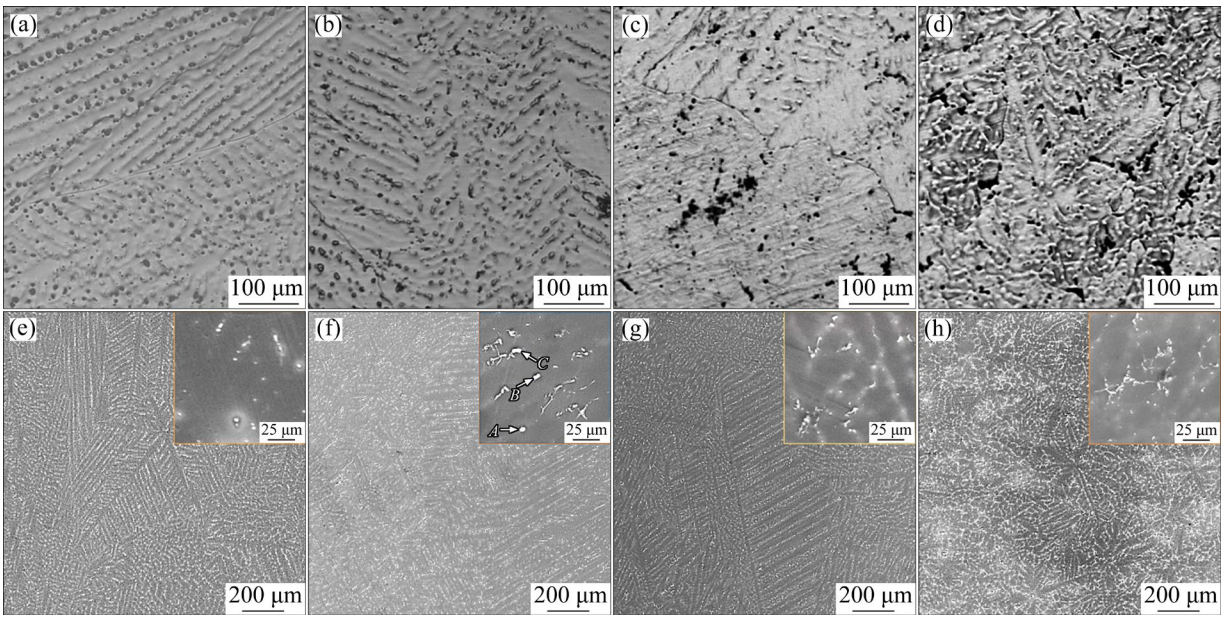

Fig. 1 OM (a−d) and SEM (e−h) images of as-cast Mg−*x*Gd−0.8Mn alloy samples: (a, e) Mg−0.8Mn alloy; (b, f) Mg−2Gd−0.8Mn alloy; (c, g) Mg−4Gd−0.8Mn alloy; (d, h) Mg−6Gd−0.8Mn alloy

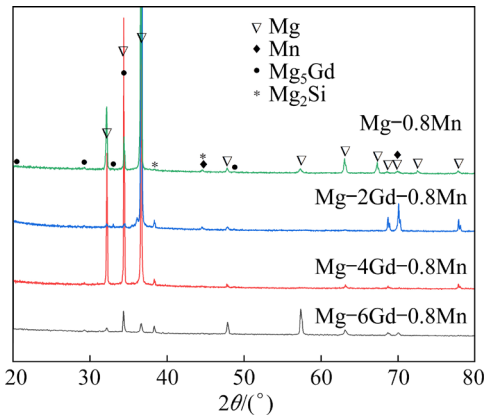

Fig. 2 XRD patterns of as-cast Mg−*x*Gd−0.8Mn alloy

blockage of grain boundary migration may only occur in a relatively small amount of second phases. Higher Gd content brings bigger size and larger quantity of the second phase, which will in turn delay the grain refinement process. In a word, greater Gd content is discovered to weaken the grain refinement effect in the alloy.

Table 2 EDS analysis results of points marked in Fig. 1(f)

Point	Content/wt.%(at.%)		
	Gd	Mn	Mg
A	11.35(1.94)	−	88.65(98.06)
B	25.29(5.01)	0.41(0.23)	74.3(94.76)
C	33.46(7.02)	−	66.58(92.80)

The extruded Mg−*x*Gd−0.8Mn alloy sheet samples were etched before SEM and EDS observations (Fig. 4 and Table 3). According to Fig. 4(a), there is a small amount of granular second

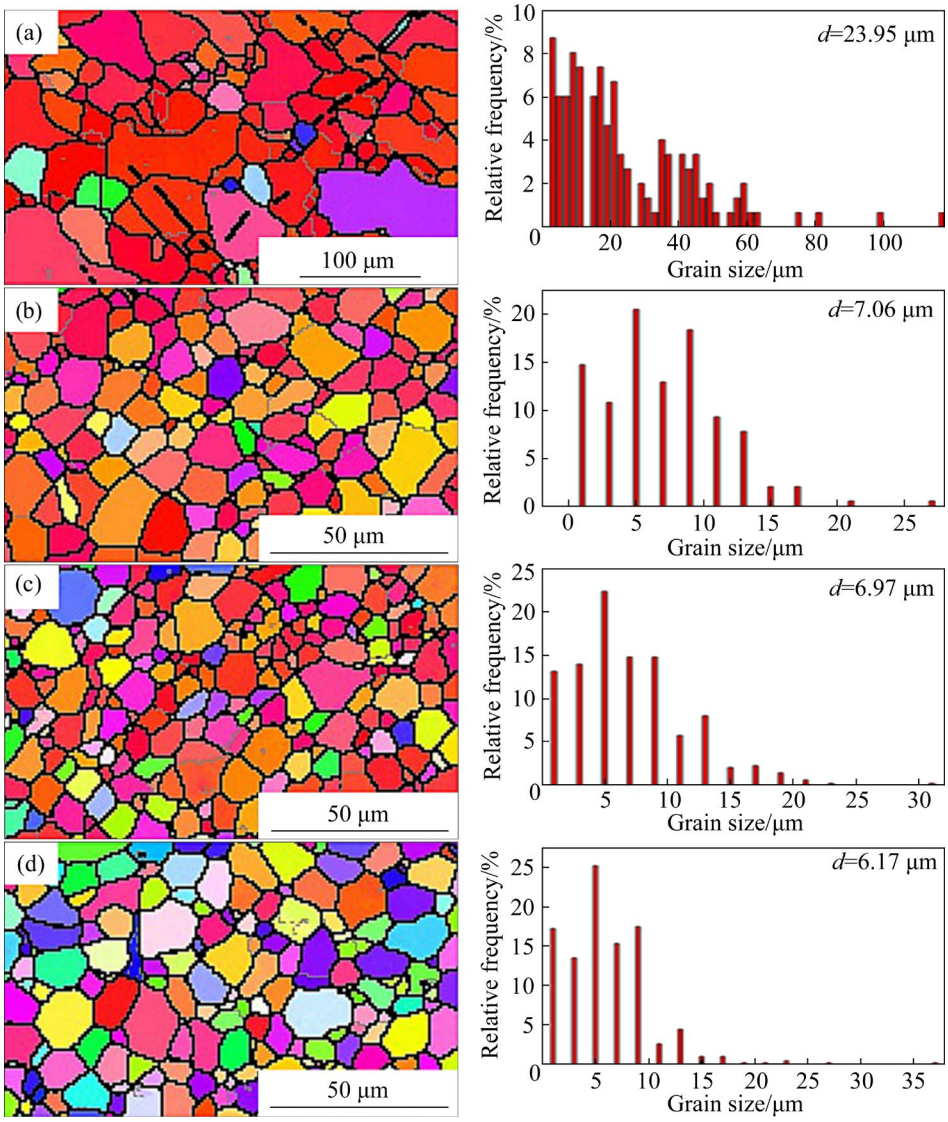

Fig. 3 Mircrograph and grain size distribution of extruded Mg−*x*Gd−0.8Mn alloys: (a) Mg−0.8Mn; (b) Mg−2Gd−0.8Mn; (c) Mg−4Gd−0.8Mn; (d) Mg−6Gd−0.8Mn

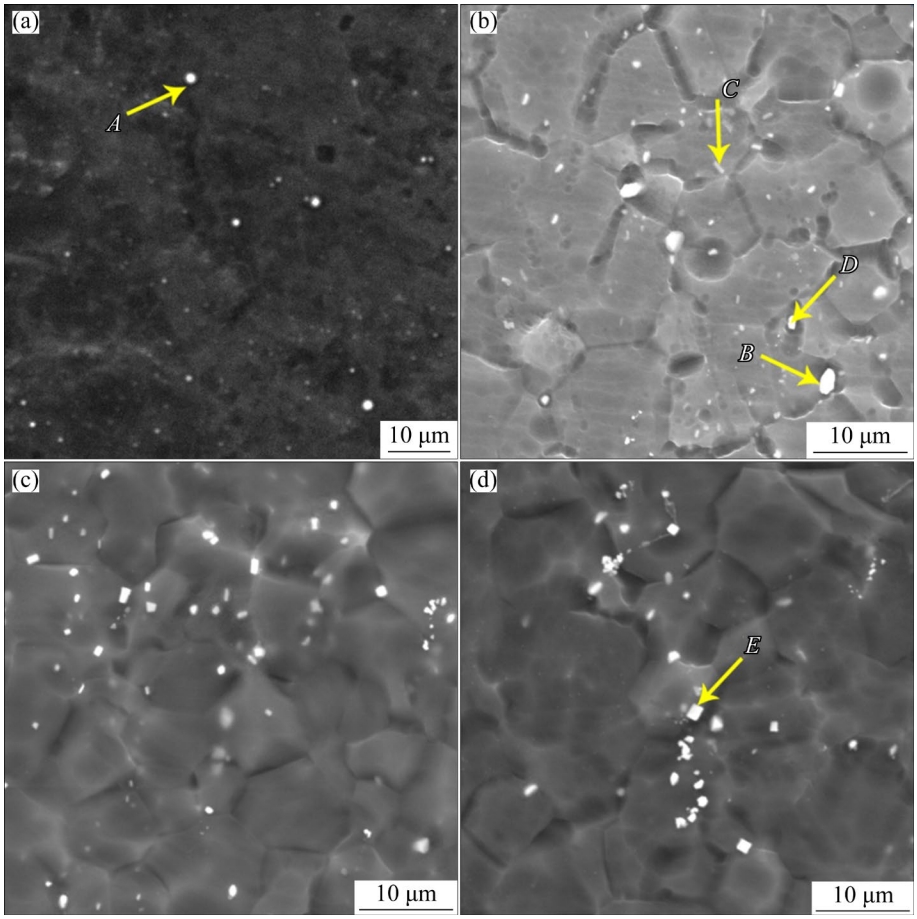

Fig. 4 SEM images of extruded Mg−*x*Gd−0.8Mn alloy sheets: (a) Mg−0.8Mn; (b) Mg−2Gd−0.8Mn; (c) Mg−4Gd−0.8Mn; (d) Mg−6Gd−0.8Mn

Table 3 EDS analysis results of points marked in Fig. 4

Point	Content/wt.%(at.%)		
	Gd	Mn	Mg
A	−	12.19(5.80)	87.81(94.20)
B	65.95(23.15)	0.37(0.38)	33.68(76.47)
C	1.86(0.31)	8.86(4.20)	89.27(95.50)
D	20.43(3.82)	0.11(0.06)	79.46(96.12)
E	48.19(12.62)	0.42(0.32)	51.39(87.06)

phase (average size ~0.76 μm) in the extruded Mg−0.8Mn alloy sheets with an area fraction below 0.1%. Based on the EDS results of Point *A* in Fig. 4(a), this second phase may be Mn. The addition of 2 wt.% Gd results in the formation of short rod-shaped and granular second phases (average size ~0.62 μm) with the area fraction increasing to 0.16%. According to EDS analysis results in Fig. 4(b), the granular Point *B*, gray dark short rod-shaped Point *C*, and bright short rod-shaped Point *D* are considered Gd-rich phase, Mn phase, and Mg_5Gd phase, respectively. As the Gd content increases to 4 wt.% and 6 wt.%, the area fraction of the second phase also rises to 0.19% and 0.51%, respectively, but these alloys show similar average size of the second phase (average size ~0.81 μm) with gradual appearance of block-like second phases. EDS results of Point *E* in Fig. 4(d) suggest that the block-like second phase is Gd-rich phase. It should be noted that Gd, Mn and Mg appear simultaneously in the second phase of the extruded alloy, indicating that Gd (or Mn) may dissolve in the Mn (or MgGd) phases.

The (0001) pole figures of the extruded Mg−*x*Gd−0.8Mn alloy sheets and the distribution tilt from ND to ED are shown in Figs. 5 and 6, respectively. According to Fig. 5(a), a typical strong basal texture in which the basal plane (0001) is parallel to the ED appears in the extruded Mg−0.8Mn alloy with a maximum texture intensity of 15.08 mrd. Following Gd addition, the texture of all the alloy sheets is turned from basal texture to the ED-split texture, and the texture intensity

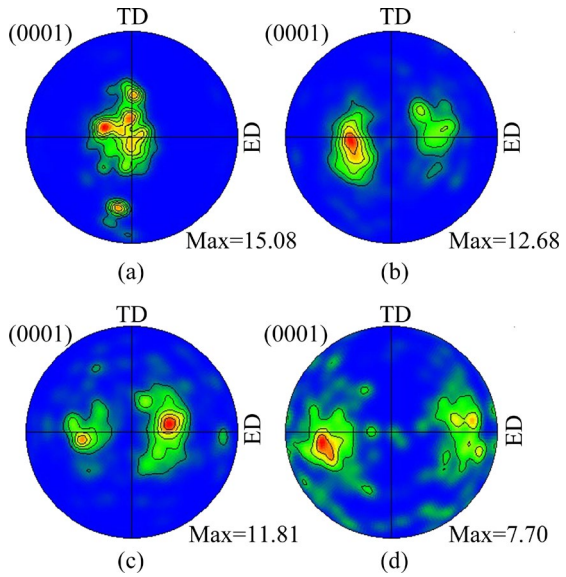

Fig. 5 (0001) pole figures of extruded Mg−*x*Gd−0.8Mn alloy: (a) Mg−0.8Mn alloy; (b) Mg−2Gd−0.8Mn alloy; (c) Mg−4Gd−0.8Mn alloy; (d) Mg−6Gd−0.8Mn alloy

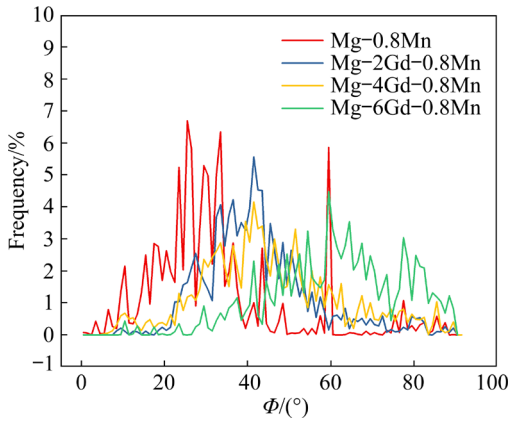

Fig. 6 Distribution of tilt from ND toward ED in (0001) pole figure

weakens. The Gd contents of 2, 4 and 6 wt.% correspond to maximum texture intensities of 12.68, 11.81 and 7.70 mrd, respectively, suggesting more apparent weakening effect of Gd as its content grows. Although there is no significant change in the texture type, higher Gd content is still correlated to higher split degree and greater maximum texture intensity. The peak angles of the extruded Mg−0.8Mn, Mg−2Gd−0.8Mn, Mg−4Gd−0.8Mn and Mg−6Gd−0.8Mn alloys are 33.5°, 41.5°, 41.5° and 59.5°, respectively.

The electrical conductivity of the extruded Mg−*x*Gd−0.8Mn alloy is depicted in Fig. 7, where the slope of the broken line is d_{IACS}/d_x that reflects the change rate of conductivity as the Gd content increases, and *x* represents the Gd content. After hot extrusion of Mg−0.8Mn alloy, only a small amount of Mn is present as a solid solution in the Mg matrix, and *α*-Mn particles precipitate from the Mg matrix, ensuring that the extruded Mg−0.8Mn alloy has a high conductivity. Following the dissolution of Gd atoms, the conductivity of the alloy falls rapidly. The extent of d_{IACS}/d_x increase when Gd content lies within 0−2 wt.% is much more significant than that with Gd content between 2−6 wt.%, indicating that Gd solute is mostly present as a solid solution state when its content is lower than 2 wt.%. When the content of Gd increases to 2−4 wt.%, d_{IACS}/d_x values are also relatively large, indicating that the solid solubility of Gd in Mg−*x*Gd−0.8Mn alloy lies within that range. However, d_{IACS}/d_x becomes small as the content of Gd exceeds 4 wt.%, where the conductivity of the alloy is mainly influenced by factors such as the second phase and grain size.

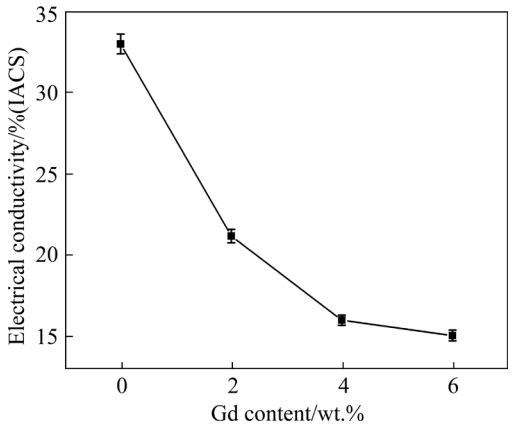

Fig. 7 Electrical conductivity of extruded Mg−*x*Gd−0.8Mn alloy

3.2 Mechanical properties

The tensile and compressive stress−strain curves of the extruded Mg−*x*Gd−0.8Mn alloy along the ED at RT are shown in Figs. 8(a) and (b). In Fig. 8 and Table 4, TYS, UTS, TFS, CYS, UCS, and CFS represent the tensile yield strength, ultimate tensile strength, tensile failure strain, compressive yield strength, ultimate compressive strength and compressive failure strain of the alloy, respectively. The tensile and compressive asymmetry of Mg alloys are quantitatively described as CYS/TYS and strength differential effect (SDE), and SDE is defined as follows [22]:

$$\mathrm{SDE}=2\times\frac{|\mathrm{CYS}|-|\mathrm{TYS}|}{|\mathrm{CYS}|+|\mathrm{TYS}|} \quad (1)$$

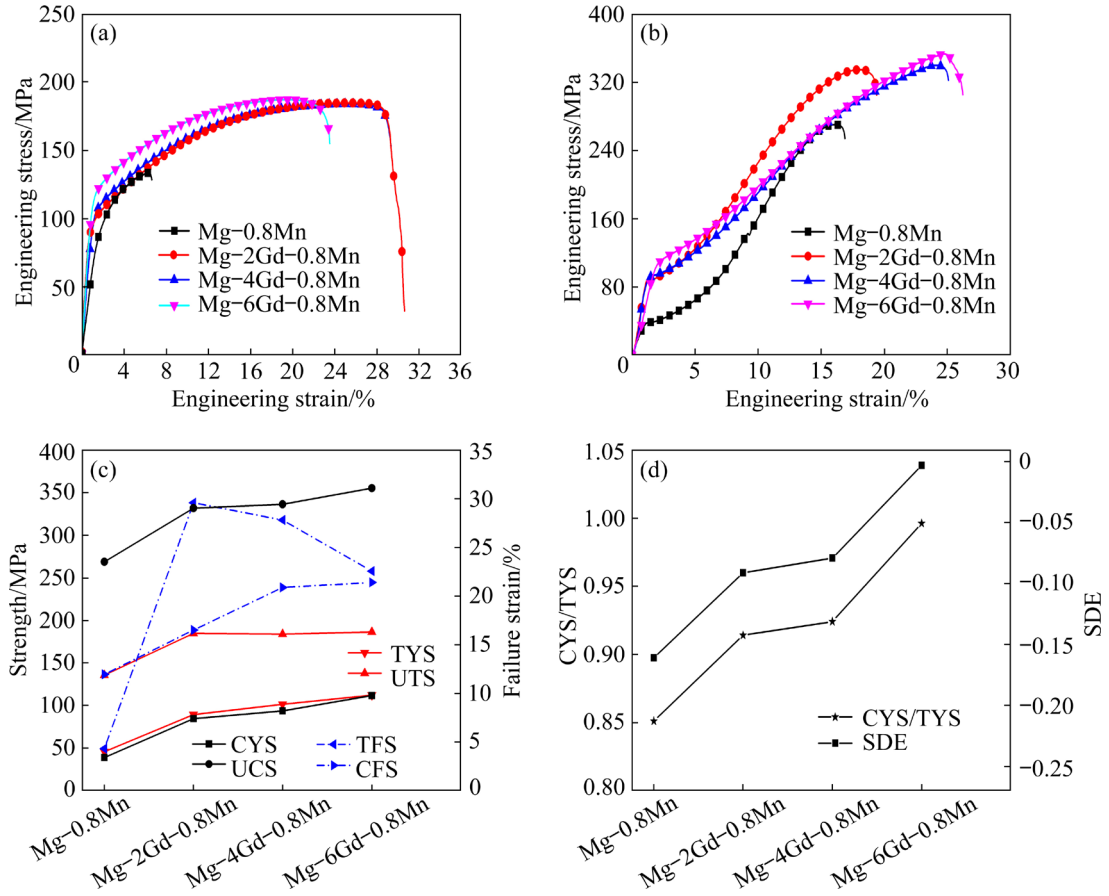

Fig. 8 Engineering tensile (a) and compressive (b) stress−strain curves of extruded Mg−*x*Gd−0.8Mn alloy along ED at RT; (c) Variation of TYS, CYS, UTS, UCS, TFS and CFS with Gd content; (d) Variation of CYS/TYS and SDE of extruded alloy

Table 4 Tensile and compressive properties of extruded Mg−*x*Gd−0.8Mn alloy along ED at RT

Alloy	Tension			Compression			CYS/TYS	SDE
	TYS/MPa	UTS/MPa	TFS/%	CYS/MPa	UCS/MPa	CFS/%		
Mg−0.8Mn	45.58±0.5	135.67±1.8	4.32±0.4	38.80±0.6	268.90±3.5	11.95±0.2	0.851	−0.161
Mg−2Gd−0.8Mn	89.21±0.8	184.74±2.2	29.60±1.3	81.5±1.0	332.01±2.6	16.51±0.7	0.914	−0.091
Mg−4Gd−0.8Mn	101.33±1.1	184.00±1.4	27.82±0.9	93.61±0.7	336.51±1.8	20.88±1.2	0.924	−0.079
Mg−6Gd−0.8Mn	112.13±0.9	186.41±1.7	22.56±0.7	111.70±1.6	355.53±3.0	21.41±0.9	0.996	−0.003

The extruded Mg−0.8Mn alloy exhibits poor mechanical properties after hot extrusion deformation. This can be attributed to an apparent gain in grain size and strong basal texture; specifically, TYS and CYS are (45.58±0.5) MPa and (38.80±0.6) MPa, and TFS and CFS are (4.32±0.4)% and (11.95±0.2)%, respectively. At Gd content of 2 wt.%, the extruded alloy shows a rapidly increase of TYS and UTS (CYS and UCS) compared to that with 0% Gd. Such growth rate for TYS and UTS (CYS and UCS) turns slower for 4 wt.% and 6 wt.% Gd, and the extruded Mg−6Gd−0.8Mn alloy demonstrates the highest TYS and UTS (CYS and UCS) of (112.13±0.9) MPa and (186.41±1.7) MPa ((111.70±1.6) MPa and (355.53±3.0) MPa), respectively. The relationship between TFS and CFS of the extruded alloy and Gd addition is shown in Fig. 8(c). TFS exhibits the highest value at 2 wt.% Gd ((29.60±1.3)%), while CFS of the extruded Mg−6Gd−0.8Mn alloy is the

highest ((21.42±0.9)%).

The relationship of CYS/TYS, SDE, and Gd content is shown in Fig. 8(d). For the extruded Mg−0.8Mn alloy, its CYS/TYS and SDE are 0.851 and −0.161, respectively, suggesting its pronounced yield asymmetry in tension and compression. As the Gd content increases to 2, 4, and 6 wt.%, CYS/TYS also grows to 0.914, 0.924 and 0.996, indicating lower anisotropy of the tensile and compressive yields in the alloy. Similarly, SDE gradually increases from −0.161 to −0.003 as the Gd content ascends from 0 to 6 wt.%. The results reveal that the tensile and compressive yield asymmetry of the alloy material falls continuously as the Gd content grows.

The fracture section and surface morphology of the extruded Mg−*x*Gd−0.8Mn alloy after the tensile test along the ED is depicted in Fig. 9. The extruded Mg−0.8Mn alloy exhibits a typical brittle intergranular fracture morphology, and some Mn particles can be observed on the cleavage step. Such morphology changes obviously when Gd is added to the alloy. Many dimples are observed on the fracture surface of the extruded Mg−2Gd−0.8Mn alloy, indicating significant plastic deformation before the alloy fractures. In addition, a bright white second phase can be found at the dimple bottom. More Gd content results in a large number of dimples as well as a certain amount of cleavage steps on the fracture surface, suggesting significant local plastic deformation before the alloy fractures. For the extruded alloy with Gd content, its fracture morphology lies between ductile fracture and brittle fracture, suggesting that the alloy has certain strength and plasticity. The surface morphology of the alloy also reveals that a certain amount of tensile twins (red mark in Figs. 9(e−h)) may start before the alloy fractures.

4 Discussion

4.1 Microstructure variation

For the as-cast Mg−*x*Gd−0.8Mn alloy, its dendrite spacing and dendrite unit area are negatively correlated with the Gd content, which may be due to solute segregation and limitations caused by densely distributed second phases near the dendrites. Literature [23,24] suggests that the growth kinetics factors for Mn and Gd are 0.15 and 1.03, respectively, which demonstrates that the refinement effect of Mn and Gd on the as-cast Mg alloys is limited. However, both MgGd and Mn phases can serve as a heterogeneous nucleation core that enhances dendrite pinning and inhibits dendrite growth.

Previous studies [25,26] have shown that modification with Mn can significantly refine the microstructure of extruded Mg alloys. However, we

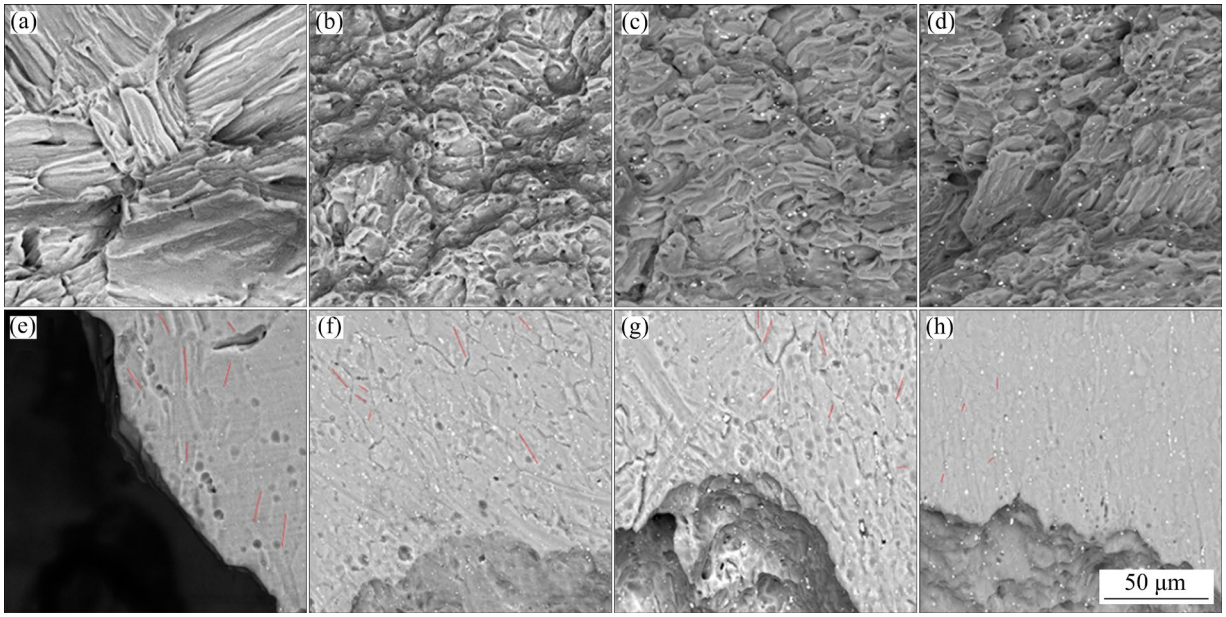

Fig. 9 SEM images showing tensile fracture surfaces of extruded Mg−*x*Gd−0.8Mn alloy: (a, e) Mg−0.8Mn alloy; (b, f) Mg−2Gd−0.8Mn alloy; (c, g) Mg−4Gd−0.8Mn alloy; (d, h) Mg−6Gd−0.8Mn alloy; (a−d) Cross section morphology; (e−h) Surface morphology

have found that the grain size of Mg−0.8Mn alloy remains prominent compared to the Mg−*x*Gd−0.8Mn alloy, which might be due to the extrusion temperature being too high at 430 °C. Extrusion at this high temperature may cause the DRXed grain growth to break through the grain boundary pinning of the second phase. According to Fig. 3, Gd addition can significantly refine the grain size in the alloy. Gd has a larger atomic radius and its grain boundary segregation can effectively reduce the mobility of these boundaries during extrusion. Besides, the area fraction of the second phase in the alloy is positively correlated to the Gd content, and these second phases can provide nucleation sites for the subsequent recrystallization [27] and grain refinement during alloy deformation.

The texture evolution with different Gd contents is displayed in Fig. 5. From the typical basal texture in the extruded Mg−0.8Mn alloy, the texture changes to a ED-split one in the extruded Mg−*x*Gd−0.8Mn alloy sheets. For more in-depth investigation of the texture evolution, all grains are divided into two parts based on different grain orientations of the alloy, in which the ND of the grain is tilted by 30° to the ED at the boundaries. Subsequently, the IPF map and corresponding reverse pole map are drawn on the ED−ND plane (Fig. 10). In this study, grains with *c*-axis tilted away from the ND for less than 30° are defined as basal texture grains, while the other grains are defined as non-basal texture grains. The strength of non-basal texture grain components (maximum texture intensity: 4.41−2.67 mrd) is weaker than the basal ones (maximum texture intensity: 18.48−12.69 mrd). The area fraction and maximum texture density of basal texture grains are both negatively correlated to the Gd content between 0 and 4 wt.%. However, at a Gd content between 4 and 6 wt.%, even though the area fraction continues to decrease, the maximum density of basal texture components abnormally rises due to the activation of non-basal slips that rotate the *c*-axis of grains to the ED direction [6,28]. Gd atoms are prone to segregation and pinning at grain boundaries, thereby inhibiting grain rotation toward the deformation direction and inducing the formation of rare earth textures. On the other hand, for non-basal texture grains, Gd content is positively correlated to its area fraction but negatively correlated to its maximum texture density, which may be attributed to the activation of additional deformation mechanisms [29]. Furthermore, particle-induced recrystallization

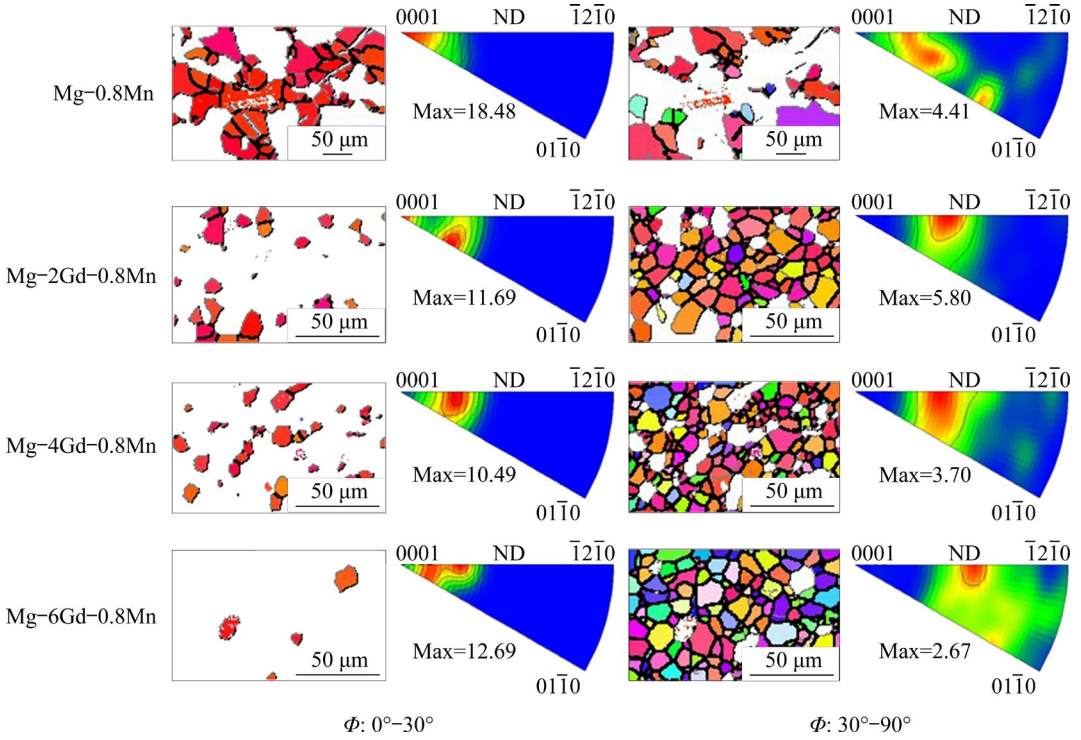

Fig. 10 EBSD IPF maps in ED−ND plane and inverse pole figures of Mg−*x*Gd−0.8Mn alloys corresponding to grains with different orientations (Distinguishing between different grain texture components is based on the deviation of 30° between the ND and the *c*-axis of grain)

nucleation mechanism (PSN) initiated by the Gd-containing second phase particles can also affect the alloy texture [30]. Even so, second phase particles in Mg−*x*Gd−0.8Mn alloys are small (size < 1 μm) with a small area fraction, suggesting that PSN during the extrusion process is negligible.

4.2 Evolution of mechanical properties

The yield strength of wrought Mg alloys is closely related to their grain size, solid solubility of the solute(s), the second phase, and the texture. Specifically, the relationship between grain size and strength of alloy materials can be expressed as the Hall−Patch formula [31]:

$$\sigma_y=\sigma_0+kd^{-1/2} \quad (2)$$

where σ_y is the yield strength of the alloy, σ_0 is the yield strength of pure Mg, k is the Hall−Petch constant, and d is the average grain size. Grain refinement can increase the number and area of grain boundaries and shorten the path for dislocation slip, thereby causing discontinuous slips at grain boundaries and boosting strength. Moreover, the coordination of deformation, such as grain rotations and grain boundary movements, is easier with grain refinement, which may therefore improve the plasticity of alloy after extrusion [32]. Generally speaking, when the grain size is within the range of several micrometers, grain refinement contributes to the initiation of non-basal slip in Mg alloys. In short, grain refinement can simultaneously improve the strength and plasticity of the alloy.

The second phase is also essential for the strength and plasticity of alloy, which may hinder the movement of dislocations and improve the alloy strength following the Orowan mechanism [33]. To be more specific, its strengthening effect is mainly determined by the area fraction and average size of the precipitation phase. In this study, the average size and area fraction of the second phase in the alloy change slightly across different Gd contents (Fig. 4), indicating that the second phase is not the main factor for improving the strength and plasticity of the alloy.

Texture is another significant factor on yield strength and plasticity of wrought Mg alloys. It is reported that the critical shear stress (CRSS) of Mg alloy basal slip at room temperature is 0.6−0.7 MPa, which is less than 1% of the CRSS of non-basal slips [34]. Therefore, basal slip is comparably easier to start slipping in wrought Mg alloys. The distribution diagram of the SF factor of basal slip in extruded Mg−*x*Gd−0.8Mn alloys under tension along the ED direction is shown in Fig. 11. For the extruded Mg−0.8Mn alloy, its basal slip has an average SF factor as low as 0.18. Higher Gd content corresponds to greater m_{basal}, indicating that the basal slip is easier to activate after Gd modification. It is reported that the yield strength/plasticity of alloy can be calculated from the SF factor of basal slip as [35]

$$\sigma_s=\tau/m_s \quad (3)$$

$$\varepsilon=\gamma m_s \quad (4)$$

where σ_s and ε represent the yield strength and plasticity of the alloy, respectively; τ is the CRSS of basal slip; γ is the shear strain; m_s is the SF factor of basal slip. The yield strength of the alloy is inversely proportional to the m_s. However, for the extruded Mg−*x*Gd−0.8Mn alloy, m_s is negatively correlated to the yield strength, indicating more significant contribution of grain refinement to the increase of yield strength compared to grain orientation. Similarly, the plasticity of the alloy is proportional to the m_s. The m_s is on the rise at 2 wt.% Gd, and the tensile failure strain is the largest up to (29.6±1.3)%, indicating that a small amount of Gd is conducive to solution plasticization [36]. However, ε falls at Gd content greater than 2 wt.% despite that m_s remains high, suggesting that more Gd atoms in the solution are not conducive to the continuous improvement of plasticity.

Judging from Table 4, the asymmetry of the tensile and compressive yield of the extruded Mg−*x*Gd−0.8Mn alloy gradually decreases with the increase of Gd content. For wrought Mg alloys, their CYS/TYS is immediately less than 1 and SDE is immediately less than 0. It is reported that the tensile twin mechanism depends more on the grain size compared to the slip mechanism; in other words, larger grain sizes tend to result in the formation of tensile twins during the tensile process [37,38]. Compared to basal slip and tensile twins, non-basal slip in the tensile process of Mg−Gd alloy may coordinate the tensile strain and improve the tensile yield strength. Besides, the activation of many tensile twins during compression will reduce the compressive yield strength of the alloy. Such

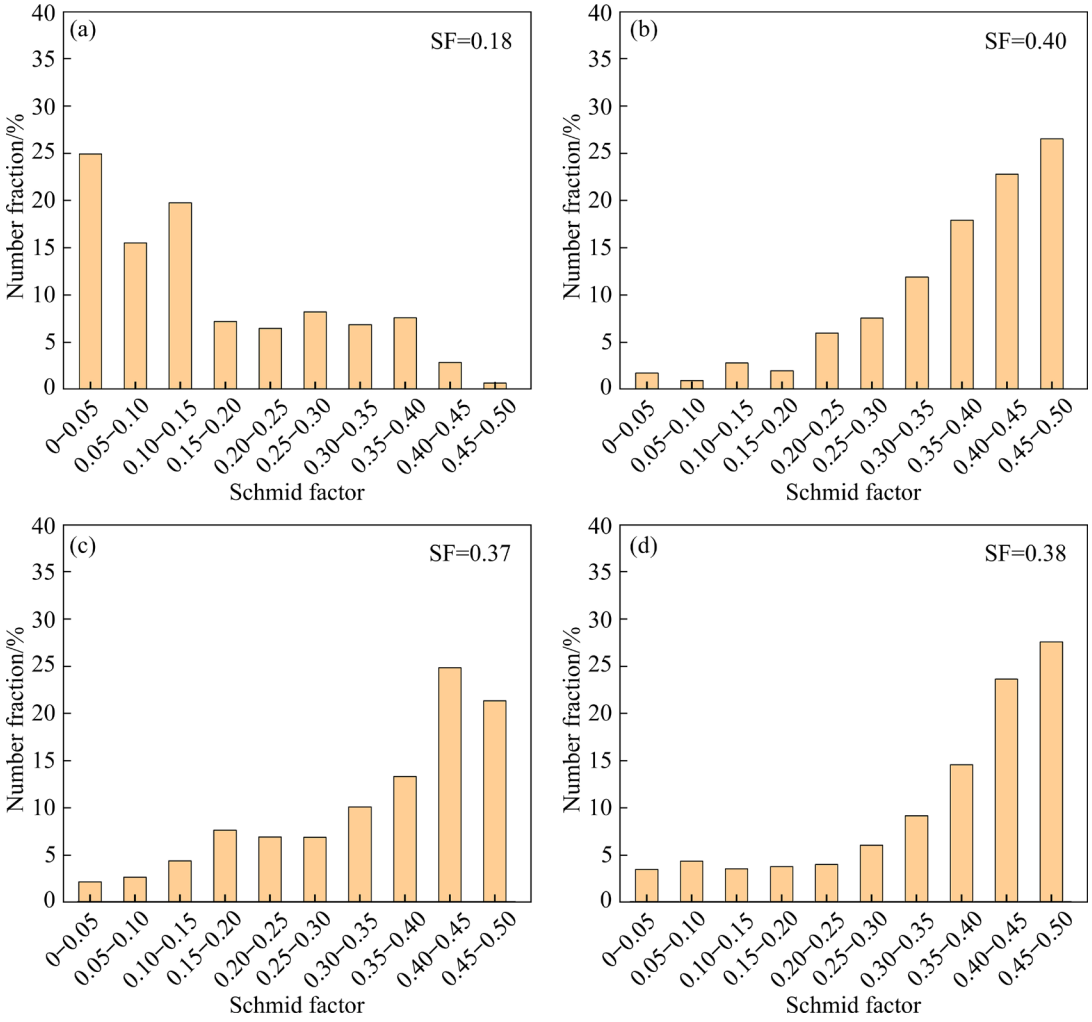

Fig. 11 SF distribution for basal slip in extruded alloy in tension (when the tensile direction is parallel to ED direction): (a) Mg−0.8Mn alloy; (b) Mg−2Gd−0.8Mn alloy; (c) Mg−4Gd−0.8Mn alloy; (d) Mg−6Gd−0.8Mn alloy

lower asymmetry of tensile and compressive yields is partly due to lower formation of tensile twins thanks to grain refinement.

To reveal the contribution of texture regulation as a result of Gd addition to the asymmetry of tensile and compressive yield, the average SF factor of $\{10\bar{1}2\}$ tensile twins compressed along the ED direction is calculated and analyzed (Fig. 12). Compared with the extruded Mg−0.8Mn alloy, the extruded Mg−2Gd−0.8Mn alloy has a higher average SF factor for the tensile twins, indicating that the latter has tensile twins that are easier to activate during alloy compression. As the Gd content continues to rise, the influence of slip, especially non-basal slip, during tension and compression accumulates. Higher Gd content corresponds to lower average SF factor between 0.4 and 0.5 in the tensile twin. At Gd content >2 wt.%, the amount of tensile twins formed during compression is reduced. On the other hand, the second phase also inhibits the nucleation and growth of tension twins. However, the second phase does not change significantly in terms of average size and area fraction with different Gd contents. Therefore, grain refinement and texture weakening following Gd addition are the main reasons for lower yield asymmetry in tension and compression.

4.3 Solid solution strengthening and plasticizing effect

The tensile test at room temperature suggests that the yield strength and plasticity of the alloy are positively correlated to Gd content within 0−2 wt.%. Specifically, 2 wt.% is the limit of Gd addition for the extruded Mg−*x*Gd−0.8Mn alloy to obtain solid solution and plasticizing effect. At Gd contents of

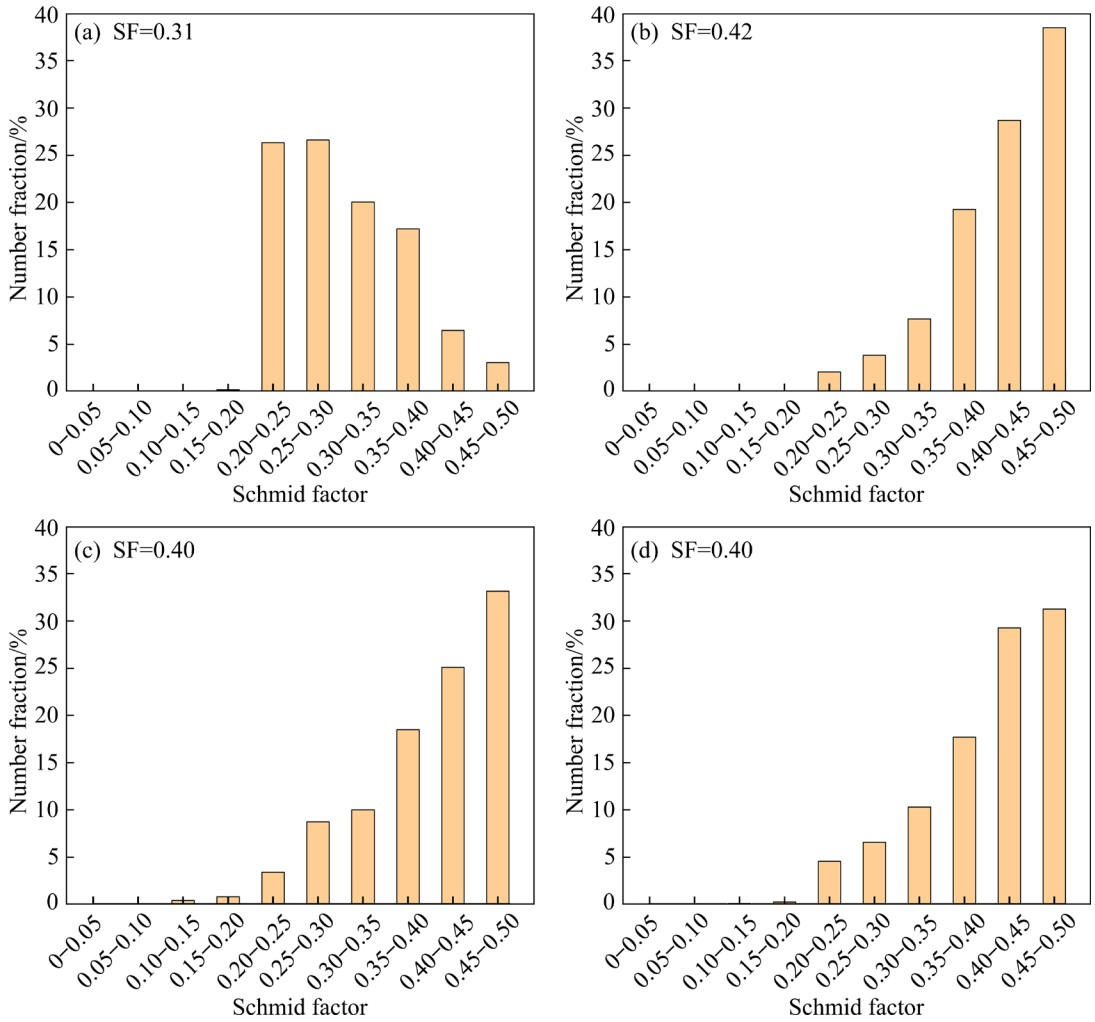

Fig. 12 SF distribution for $\{10\bar{1}2\}$ tensile twins in extruded alloy under compression: (a) Mg−0.8Mn alloy; (b) Mg−2Gd−0.8Mn alloy; (c) Mg−4Gd−0.8Mn alloy; (d) Mg−6Gd−0.8Mn alloy

2−6 wt.%, the alloy exhibits continuously growing strength but falling plasticity. In short, the combination of solid solution strengthening and plasticization effect of the extruded Mg−*x*Gd−0.8Mn alloy mainly occurs when Gd content is between 0 and 2 wt.%.

Previous research [39] concluded that Gd atoms in dilute Mg−Gd binary alloy prefer to locate on the prismatic plane, and the solid solution strengthening and plasticizing effect of Mg−Gd alloy mainly occurs in the composition range of 1−4 wt.% Gd. Addition of Mn can help effectively to remove inclusions such as Fe in the melt [20,21] and preserve rare earth Gd during inclusion removal and improve the atomic utilization of Gd in the alloy [17]. Compared with the extruded Mg−Gd alloy, the actual solid solubility of Gd in Mg−*x*Gd−0.8Mn alloy is higher. In other words, the limit of Gd addition to obtain solid solution strengthening and plasticizing effect after Mn addition is reduced from 4 to 2 wt.%, which is of significant theoretical value for developing Mg alloys with low Gd content and high plasticity.

The vast majority of Mn atoms in Mg−*x*Gd−0.8Mn alloy precipitates during hot extrusion, which means that the changing trend of the solid solution substitutional position of Gd atoms in Mg−*x*Gd and Mg−*x*Gd−0.8Mn alloys is consistent with the increase of Gd content as long as the addition amount is within the solid solubility. Similarly, the trend of basal slip and prismatic slip resistance of extruded Mg−*x*Gd−0.8Mn alloy can be predicted (Fig. 13). The alloy basal slip exhibits sharp increase in its starting resistance when Gd content is low (0−2 wt.%), but the starting resistance of prismatic slip goes up slowly and

steadily. Therefore, the difference between these two resistances will inevitably reach a certain degree with higher Gd content, which is conducive to the coordinated basal slip and prismatic slip and may boost the strength and plasticity of alloys. However, at a certain Gd content, the volume fraction and distribution characteristics of the alloy's second phase may change and adversely affect plasticity.

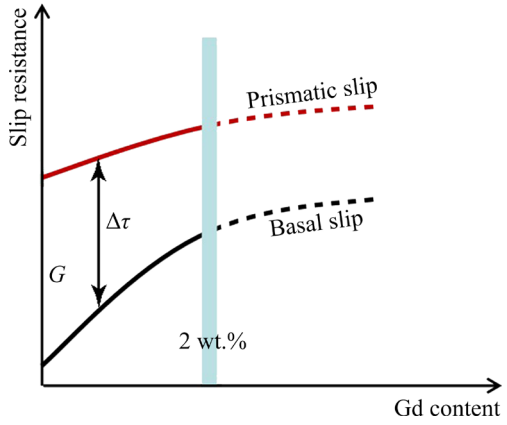

Fig. 13 Prediction diagram of basal slip and prismatic slip starting resistance CRSS varying with Gd content

5 Conclusions

(1) Gd has a strong grain refinement effect on the extruded Mg−*x*Gd−0.8Mn alloy. Higher Gd content would lead to lower area fraction of basal texture grains and higher area fraction of non-basal texture grains, and both grains may show lower maximum density. However, at a Gd content of 6 wt.%, the maximum density of the basal texture component abnormally increases, which is mainly attributed to the activated non-basal slips that rotate the *c*-axis of grains to the ED direction.

(2) As the Gd content grows from 0 to 6 wt.%, the asymmetry of the tensile and compressive yields of the extruded Mg−*x*Gd−0.8Mn alloy decreases as identified by increasing CYS/TYS (from 0.851 to 0.996) and SDE (from −0.161 to −0.003). The main reasons for such reduction in yield asymmetry include grain refinement and texture weakening.

(3) The solid solution strengthening and plasticizing effect of the extruded Mg−*x*Gd−0.8Mn alloy mainly occurs in the composition range of 0−2 wt.%, and the contribution of grain refinement to higher alloy yield strength is more significant than that of grain orientation. Compared with the extruded Mg−*x*Gd alloy, the limit of Gd addition to obtain solid solution strengthening and plasticizing effect after Mn addition is reduced from 4 to 2 wt.%.

CRediT authorship contribution statement

Dong-dong GU: Writing-original draft, Investigation, Data curation; **Jian PENG:** Writing − Review & editing, Validation, Supervision, Resources, Project administration, Investigation, Funding acquisition, Conceptualization; **Fu-sheng PAN:** Resources, Funding acquisition, Conceptualization.

Declaration of competing interest

The authors declare that they have no known competing financial interests or personal relationships that could have appeared to influence the work reported in this paper.

Acknowledgments

This work was supported by the National Natural Science Foundation of China (No. U2241231), National Key Research and Development Program of China (No. 2021YFB3701100), Scientific Research Project of Jiangxi Provincial Department of Education, China (No. GJJ211038), and Doctoral Research Project of Jinggangshan University, China (No. JZB2110).

References

[1] FENG Yun, ZHANG Ze, WEN Liang-yuan, XU Yu-zhao, LI Jia-qi, LI Jing-yuan. Investigating the potential applications of Mg−Zn−Y−Gd−Mn alloy biodegradable implants in the field of orthopedics [J]. Materials Letters, 2023, 343, 134330.

[2] JIANG Bin, DONG Zhi-hua, ZHANG Ang, SONG Jiang-feng, PAN Fu-sheng. Recent advances in micro-alloyed wrought magnesium alloys: Theory and design [J]. Transactions of Nonferrous Metals Society of China, 2022, 32(6): 1741−1780.

[3] SONG Jiang-feng, SHE Jia, CHEN Dao-lun, PAN Fu-sheng. Latest research advances on magnesium and magnesium alloys worldwide [J]. Journal of Magnesium and Alloys, 2020, 8: 1−41.

[4] PAN Xiao-huan, WANG Li-fei, LU Peng-bin, ZHANG Hua, HUANG Guang-sheng, ZHENG Liu-wei, XING Bin, CHENG Wei-li, WANG Hong-xia, LIANG Wei, SHIN K S. Unveiling the planar deformation mechanisms for improved formability in pre-twinned AZ31 Mg alloy sheet at warm temperature [J]. Journal of Magnesium and Alloys, 2023, 11(12): 4659−4678.

[5] WU Z, CURTIN W A. The origins of high hardening and low ductility in magnesium [J]. Nature, 2015, 526: 62−67.

[6] KIM S H, JUNG J G, YOU B S, PARK S H. Microstructure and texture variation with Gd addition in extruded

magnesium [J]. Journal of Alloys and Compounds, 2017, 695: 344−350.

[7] WANG Xue-zhao, WANG You-qiang, NI Chen-bing, FANG Yu-xin, YU Xiao, ZHANG Ping. Effect of Gd content on microstructure and dynamic mechanical properties of solution-treated Mg−*x*Gd−3Y−0.5Zr alloy [J]. Transactions of Nonferrous Metals Society of China, 2022, 32(7): 2177−2189.

[8] LEE S W, KIM S H, JO W K, HONG W H, KIM W, MOON B G, PARK S H. Twinning and slip behaviors and microstructural evolutions of extruded Mg−1Gd alloy with rare-earth texture during tensile deformation [J]. Journal of Alloys and Compounds, 2019, 791: 700−710.

[9] WANG Cheng, ZHANG Hua-yuan, WANG Hui-yuan, LIU Guo-jun, JIANG Qi-chuan. Effects of doping atoms on the generalized stacking-fault energies of Mg alloys from first-principles calculations [J]. Scripta Materialia, 2013, 69: 445−448.

[10] BARRETT C D, IMANDOUST A, ELKADIRI H. The effect of rare earth element segregation on grain boundary energy and mobility in magnesium and ensuing texture weakening [J]. Scripta Materialia, 2018, 146: 46−50.

[11] HU Yao-bo, DENG Juan, ZHAO Chong, PAN Fu-sheng, PENG Jian. Microstructure and mechanical properties of Mg−Gd−Zr alloys with low gadolinium contents [J]. Journal of Materials Science, 2011, 46: 5838−5846.

[12] HU Yao-bo, ZHANG Chao, ZHENG Tian-xu, PAN Fu-sheng, TANG Ai-tao. Strengthening effects of Zn addition on an ultrahigh ductility Mg−Gd−Zr magnesium alloy [J]. Materials, 2018, 11(10): 1942.

[13] WANG Chong, LI Hong-rui, GUO En-yu, WANG Xue-jian, KANG Hui-jun, CHEN Zong-ning, WANG Tong-min. The effect of Gd on the microstructure evolution and mechanical properties of Mg−4Zn−0.6Ca alloy [J]. Materials Science and Engineering A, 2023, 868: 144756.

[14] LEI Bin, DONG Zhi-hua, YANG Yan, JIANG Bin, YUAN Ming, YANG Hua-bao, WANG Qing-hang, HUANG Guang-sheng, SONG Jiang-feng, ZHANG Ding-fei, PAN Fu-sheng. Influence of Zn on the microstructure and mechanical properties of Mg−Gd−Zr alloy [J]. Materials Science and Engineering A, 2022, 843: 143136.

[15] ZHAO Jun, JIANG Bin, YUAN Yuan, TANG Ai-tao, WANG Qing-hang, YANG Tian-hao, HUANG Guang-sheng, ZHANG Ding-fei, PAN Fu-sheng. Influence of Ca and Zn synergistic alloying on the microstructure, tensile properties and strain hardening of Mg−1Gd alloy [J]. Materials Science and Engineering A, 2020, 785: 139344.

[16] HARMUTH J, WIESE B, BOHLEN J, EBEL T, WILLUMEIT-RÖMER R. Wide range mechanical customization of Mg−Gd alloys with low degradation rates by extrusion [J]. Frontiers in Materials, 2019, 6: 201.

[17] GU Dong-dong, PENG Jian, WANG Jia-wen, PAN Fu-sheng. Effect of Mn modification on microstructure and mechanical properties of magnesium alloy with low Gd content [J]. Metals and Materials International, 2021, 27(6): 1483−1492.

[18] WIESE B, HARMUTH J, WILLUMEIT-RÖMER R, BOHLEN J. Property variation of extruded Mg−Gd alloys by Mn addition and processing [J]. Crystals, 2022, 12: 1036.

[19] PENG Peng, TANG Ai-tao, SHE Jia, ZHANG Jian-yue, ZHOU Shi-bo, SONG Kai, PAN Fu-sheng. Significant improvement in yield stress of Mg−Gd−Mn alloy by forming bimodal grain structure [J]. Materials Science and Engineering A, 2021, 803: 140569.

[20] CAMPOS M D R S, SCHARNAGL N, BLAWERT C, KAINER K U. Improving corrosion resistance of Mg10Gd alloy [J]. Materials Science Forum, 2013, 765: 673−677.

[21] CHEN Tao, YUAN Yuan, LIU Ting-ting, LI Da-jian, PAN Fu-sheng. Effect of Mn addition on melt purification and Fe tolerance in Mg alloys [J]. JOM, 2021, 73: 892−902.

[22] SHI Feng-jian, PIAO Nan-ying, WANG Hao, WANG Ji-heng, ZANG Qian-hao, GUO Yu-hang, CHEN Cai, ZHANG Lu. Investigation of microstructure and mechanical properties of ZK60 magnesium alloy achieved by extrusion-shearing process [J]. Journal of Materials Research and Technology, 2023, 25: 799−811.

[23] HAN Qing-you. The role of solutes in grain refinement of hypoeutectic magnesium and aluminum alloys [J]. Journal of Magnesium and Alloys, 2022, 10(7): 1846−1856.

[24] YU Zheng-wen, TANG Ai-tao, WANG Qin, GAO Zheng-yuan, HE Jie-jun, SHE Jia, SONG Kai, PAN Fu-sheng. High strength and superior ductility of an ultra-fine grained magnesium-manganese alloy [J]. Materials Science and Engineering A, 2015, 648: 202−207.

[25] YU Zheng-wen, TANG Ai-tao, HE Jie-jun, GAO Zheng-yuan, SHE Jia, LIU Jian-guo, PAN Fu-sheng. Effect of high content of manganese on microstructure, texture and mechanical properties of magnesium alloy [J]. Materials Characterization, 2018, 136: 310−317.

[26] LI C C, XIA Z H, QIAO X G, GOLOVIN I S, ZHENG M Y. Superior ductility Mg−Mn extrusion alloys at room temperature obtained by controlling Mn content [J]. Materials Science and Engineering A, 2023, 869: 144508.

[27] JIANG M G, XU C, YAN H, FAN G H, NAKATA T, LAO C S, CHEN R S, KAMADO S, HAN E H, LU B H. Unveiling the formation of basal texture variations based on twinning and dynamic recrystallization in AZ31 magnesium alloy during extrusion [J]. Acta Materialia, 2018, 157: 53−71.

[28] XU Yu-ling, HUANG Yuan-ding, ZHONG Zheng-ye, YOU Si-hang, GAN Wei-min, XIAO Bi-quan, MAAWAD E, SCHELL N, GENSCH F, PAN Fu-sheng, HORT N. In situ compressive investigations on the effects of solid solution Gd on the texture and lattice strain evolution of Mg [J]. Materials Science and Engineering A, 2020, 774: 138938.

[29] BARNETT M R, NAVE M D, BETTLES C J. Deformation microstructures and textures of some cold rolled Mg alloys [J]. Materials Science and Engineering A, 2004, 386(1/2): 205−211.

[30] ROBSON J D, HENRY D T, DAVIS B. Particle effects on recrystallization in magnesium−manganese alloys: Particle-stimulated nucleation [J]. Acta Materialia, 2009, 57(9): 2739−2747.

[31] WANG Yi, CHOO H. Influence of texture on Hall−Petch relationships in an Mg alloy [J]. Acta Materialia, 2014, 81: 83−97.

[32] MALEKI M, BERNDORF S, MOHAMMADZEHI S, MIRZADEH H, EMAMY M, ULLMANN M, PRAHL U. Grain refinement and improved mechanical properties of Mg−4Zn−0.5Ca−0.5RE magnesium alloy by thermo-

mechanical processing [J]. Journal of Alloys and Compounds, 2023, 954: 170224.
[33] BARNETT M R, WANG H, GUO T T. An Orowan precipitate strengthening equation for mechanical twinning in Mg [J]. International Journal of Plasticity, 2019, 112: 108−122.
[34] KIM K H, JEON J B, KIM N J, LEE B J. Role of yttrium in activation of ⟨*c*+*a*⟩ slip in magnesium: An atomistic approach [J]. Scripta Materialia, 2015, 108: 104−108.
[35] VALLE J A D, CARREÑO F, RUANO O A. Influence of texture and grain size on work hardening and ductility in magnesium-based alloys processed by ECAP and rolling [J]. Acta Materialia, 2006, 54: 4247−4259.
[36] SHI D F, CEPEDA-JIMÉNEZ C M, PÉREZ-PRADO M T. The relation between ductility at high temperature and solid solution in Mg alloys [J]. Journal of Magnesium and Alloys, 2022, 10(1): 224−238.
[37] MEYERS M A, VÖHRINGER O, LUBARDA V A. The onset of twinning in metals: A constitutive description [J]. Acta Materialia, 2001, 49: 4025−4039.
[38] FAN H D, AUBRY S, ARSENLIS A, EL-AWADY J A. Grain size effects on dislocation and twinning mediated plasticity in magnesium [J]. Scripta Materialia, 2016, 112: 50−53.
[39] GU Dong-dong, PENG Jian, SUN Song, PAN Fu-sheng. On the solid solution substitutional position and properties of Mg−Gd alloy [J]. Journal of Materials Research and Technology, 2022, 20: 2859−2871.

低 Gd+Mn 添加对 Mg−Gd−Mn 合金显微组织和力学性能演变的协同作用

古东懂[1,2]，彭 建[1]，潘复生[1]

1. 重庆大学 材料科学与工程学院 国家镁合金材料工程技术研究中心，重庆 400044；
2. 井冈山大学 机电工程学院，井冈山 343009

摘 要：研究低 Gd+Mn 添加对 Mg−*x*Gd−0.8Mn 合金显微组织和力学性能演变的协同作用。Gd 添加对挤压态 Mg−*x*Gd−0.8Mn 合金具有强烈的晶粒细化作用，并导致合金基面织构晶粒的面积分数和相应织构组分的最大密度不断降低。然而，随着 Gd 含量增加至 6%(质量分数)，基面织构组分的最大密度急剧增加。当 Gd 含量低于 6%时，由于晶粒细化和织构弱化，合金的拉压屈服不对称性与 Gd 含量呈负相关。此外，晶粒细化对合金屈服强度提高的贡献比晶粒取向更显著。与挤压态 Mg−*x*Gd 合金相比，挤压态 Mg−*x*Gd−0.8Mn 合金显示出与固溶强化增塑效应相对应的更低的极限成分点(2%和 4%)。最后，预测了挤压态 Mg−*x*Gd−0.8Mn 合金基面滑移和柱面滑移阻力的变化趋势。

关键词：Mg−Gd−Mn 合金；Gd+Mn 添加；力学性能；织构演变；固溶强化增塑效应

(Edited by Xiang-qun LI)